

LETTER TO THE EDITOR

## The 33 M<sub>⊙</sub> black hole *Gaia* BH3 is part of the disrupted ED-2 star cluster

E. Balbinot<sup>1,2</sup>, E. Dodd<sup>1</sup>, T. Matsuno<sup>3</sup>, C. Lardo<sup>4</sup>, A. Helmi<sup>1</sup>, P. Panuzzo<sup>5</sup>, T. Mazeh<sup>6</sup>, B. Holl<sup>7,8</sup>, E. Caffau<sup>5</sup>, A. Jorissen<sup>9</sup>, C. Babusiaux<sup>10</sup>, P. Gavras<sup>11</sup>, Ł. Wyrzykowski<sup>12</sup>, L. Eyer<sup>7</sup>, N. Leclerc<sup>5</sup>, A. Bombrun<sup>13</sup>, N. Mowlavi<sup>7</sup>, G.M. Seabroke<sup>14</sup>, I. Cabrera-Ziri<sup>3</sup>, T. M. Callingham<sup>1</sup>, T. Ruiz-Lara<sup>16,17</sup>, and E. Starkenburg<sup>1</sup>

(Affiliations can be found after the references)

Received April 25, 2024; accepted ...

### ABSTRACT

**Context.** The *Gaia* Collaboration has recently reported the detection of a 33 M<sub>⊙</sub> black hole in a wide binary system located in the Solar neighbourhood.

**Aims.** Here we explore the relationship between this black hole, known as *Gaia* BH3, and the nearby ED-2 halo stellar stream.

**Methods.** We study the orbital characteristics of the *Gaia* BH3 binary and present measurements of the chemical abundances of ED-2 member stars derived from high-resolution spectra obtained with the VLT.

**Results.** We find that the Galactic orbit of the *Gaia* BH3 system and its metallicity are entirely consistent with being part of the ED-2 stream. The characteristics of the stream, particularly its negligible spread in metallicity and in other chemical elements as well as its single stellar population, suggest that it originated from a disrupted star cluster of low mass. Its age is comparable to that of the globular cluster M92 that has been estimated to be as old as the Universe.

**Conclusions.** This is the first black hole unambiguously associated with a disrupted star cluster. We infer a plausible mass range for the cluster to be relatively narrow, between 2 × 10<sup>3</sup> M<sub>⊙</sub> and 4.2 × 10<sup>4</sup> M<sub>⊙</sub>. This implies that the black hole could have formed directly from the collapse of a massive very-metal-poor star, but that the alternative scenario of binary interactions inside the cluster environment also deserves to be explored.

**Key words.** Stars: black holes – Stars: Population II – Stars: abundances – Galaxy: kinematics and dynamics – Galaxy: halo – globular clusters

### 1. Introduction

The discovery of a 33 M<sub>⊙</sub> black hole (BH) was recently reported in the *Gaia* DR4 pre-release data ([Gaia Collaboration: Panuzzo et al. 2024](#)). This BH is in a wide binary system with a period of 11.6 years. Its visible companion (*Gaia* DR3 source\_id 4318465066420528000) is a known high-proper motion star that is part of the Galactic halo. The low metallicity [Fe/H] = −2.56 ± 0.12 reported by [Gaia Collaboration: Panuzzo et al. \(2024\)](#) confirms the association with this Galactic component.

This discovery is especially exciting in light of the enormous advances made in the field of gravitational waves in recent years. Several tens of detections of gravitational waves due to merging binary BHs have been reported by the LIGO/VIRGO/KAGRA collaboration ([Abbott et al. 2023a](#)). The modelling of these events has revealed that the binary BH mass distribution follows a power-law, with peaks at chirp masses of 8 M<sub>⊙</sub> and 28 M<sub>⊙</sub> ([Abbott et al. 2023b](#)). The origin of the heavier BHs is not well understood. Because very massive stars of solar metallicity lose much of their mass via stellar winds, it has been argued that many of these BH could reside in metal-poor environments such as dwarf galaxies. An alternative pathway could be dynamical interactions in dense star clusters which may lead to hierarchical growth of BH via BH binary mergers (see e.g. [Antonini & Gieles 2020](#); [Fragione & Rasio 2023](#)). In this context, it is important to shed more light on the origin of *Gaia* BH3.

Since *Gaia* BH3 has a very retrograde and relatively loosely bound orbit, [Gaia Collaboration: Panuzzo et al. \(2024\)](#) have argued for a possible association with the Sequoia accretion event ([Myeong et al. 2019](#)) identified using *Gaia* DR2 data. The better astrometry available in the subsequent *Gaia* (E)DR3, has however revealed that this region of integrals of motion (IoM) space,

e.g. energy and angular momenta, contains several additional substructures besides Sequoia (e.g. [Ruiz-Lara et al. 2022](#); [Dodd et al. 2023](#)). Some of these substructures appear to have distinct chemistry ([Matsuno et al. 2019](#); [Naidu et al. 2020](#)).

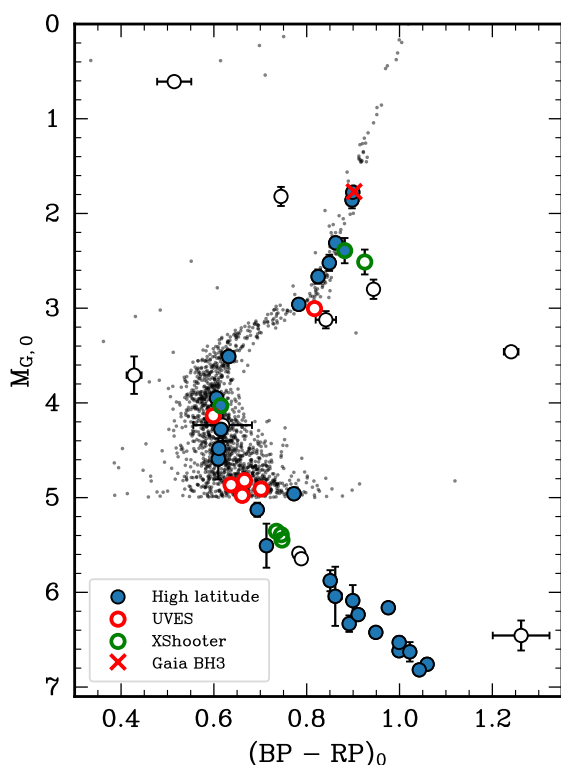
Among the smaller of such retrograde structures first identified by [Dodd et al. \(2023\)](#) we highlight ED-2. This substructure has been shown to form a dynamically cold stellar stream crossing the solar neighbourhood ([Balbinot et al. 2023](#), B23). Because of the dynamical properties of ED-2 (a cold but relatively wide stream) it was suggested that it could have originated from an ultra-faint dwarf galaxy. On the other hand, the tight distribution of its member stars in color-magnitude space and the relatively narrow (rms ≈ 0.2 dex) metallicity distribution measured from LAMOST DR3 low resolution spectra ([Li et al. 2018](#)) for 7 stars, favoured a star cluster origin. Interestingly the mean metallicity of ED-2 stars is [Fe/H] = −2.60<sup>+0.20</sup><sub>−0.21</sub>, suspiciously close to that of the companion of *Gaia* BH3.

In this Letter we demonstrate that *Gaia* BH3 is indeed associated with the cold stellar stream ED-2 and that ED-2 stems from a low-mass disrupted star cluster. Sec. 2 focuses on the dynamical association of *Gaia* BH3 with ED-2, and Sec. 3 presents chemical abundances from follow-up X-Shooter and UVES spectra of ED-2 members<sup>1</sup>. In Sec. 4 we discuss the implications of our findings and in Sec. 5 we present our conclusions.

<sup>1</sup> These data had been requested in proposals 0111.D-0263(A) (PI:Dodd) and 112.25ZW.001 (PI:Balbinot), and hence submitted before the analyses that led to the discovery of *Gaia* BH3. The co-Is of both proposals are co-authors of this paper who are not members of the *Gaia* collaboration.

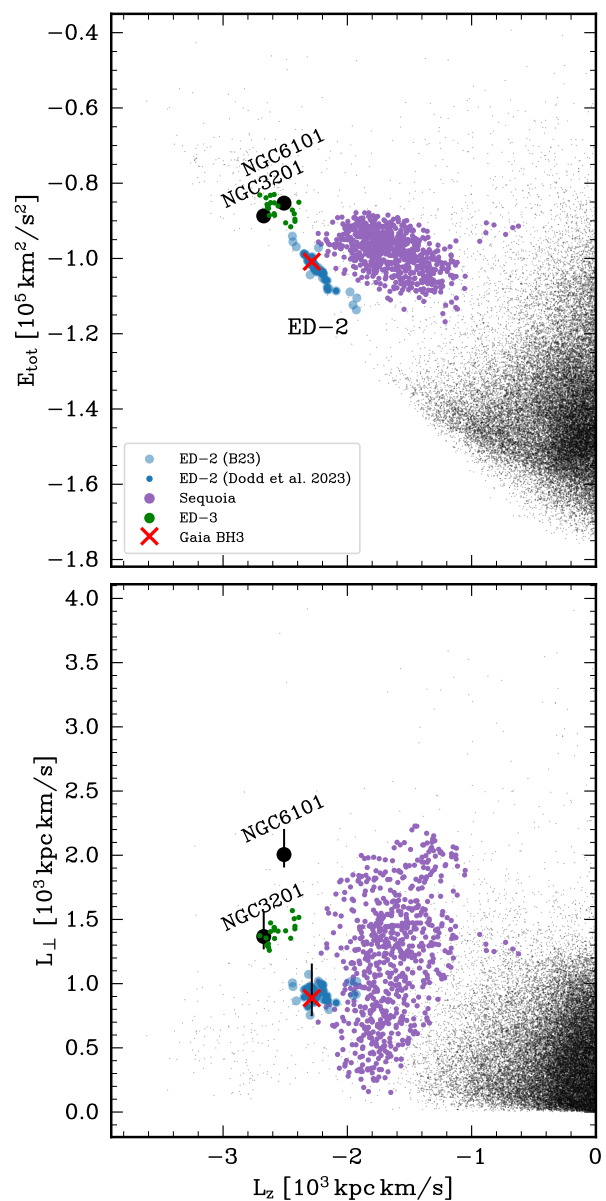
## 2. Kinematics and stellar population

Fig. 2 shows the extinction corrected colour-magnitude diagram (CMD) for all ED-2 members (see B23 for details). The cross indicates the location of the *Gaia* BH3 companion star, (which due to the high RUWE value reported in *Gaia* (E)DR3, was left out of the analysis by Dodd et al. 2023). The error bars in this figure account for the effects of distance and extinction uncertainty. All ED-2 known member stars are within 2.5 kpc from the Sun and their relative distance errors are smaller than 20%. We compute the extinction at  $d = 3 \epsilon_d$  (where  $\epsilon_d$  is the distance error) to conservatively estimate the error introduced in the 3D extinction maps of Lallement et al. (2022). These uncertainties are summed in quadrature with the photometric uncertainty. For comparison, we also plot members of the globular cluster M92 in the background. These were selected using the method of Vasiliev & Baumgardt (2021) and are at least  $4^{\circ}$  away from the M92's centre, to avoid crowding. The CMD of M92 has been extinction corrected following the recipe described above.



**Fig. 1.** *Gaia* DR3 extinction corrected CMD showing the location of the *Gaia* BH3 companion (red cross) and ED-2 members (B23) as blue and empty circles. The former are high-latitude ( $|b| > 20^{\circ}$ ), low-extinction ( $E(B - V) = 0.01$ ) ED-2 members. Notice the extremely tight sequence followed by ED-2 stars, indicative of their small metallicity dispersion. Their distribution is in very good agreement with the CMD of stars in the globular cluster M92 (truncated at  $M_{G,0} = 5$ ), shown in the background as black dots. This implies that they are of similar age, given their comparable metallicities. The object with  $M_{G,0} = 0.6$  is an RR Lyrae type-c star (Clementini et al. 2023).

This comparison shows that ED-2 stars match well the CMD of M92, which is known to be one of the oldest and most metal-poor ( $[Fe/H] = -2.3$ ) globular clusters (GC) in the Galaxy (Ying et al. 2023), with an age of  $13.80 \pm 0.75$  Gyr. Since the main-sequence turn-off (MSTO) seems to be slightly fainter, ED-2 could potentially be even older, however, this is supported by



**Fig. 2.**  $L_z$  vs.  $E_{tot}$  (top panel) and vs.  $L_{\perp}$  (bottom panel) showing ED-2 as blue and lighter blue circles, corresponding respectively to original members from Dodd et al. (2023) and to the extended sample (see B23 for details). *Gaia* BH3 is shown as a red cross. Members of ED-3 and Sequoia (as classified by Dodd et al. 2023) are also shown. The dark points in the background are from the *Gaia* DR3 6D sample within 3 kpc and  $RUWE < 1.4$ . We also show two retrograde GCs. The vertical errorbars show the variation in  $L_z$  for ED-2 and the two GCs along their orbits.

only a single MSTO star in ED-2. In any case, we may conclude from this comparison that ED-2 formed more than 13 Gyr ago.

Figure 2 shows the distribution of ED-2 stars in IoM space:  $z$ -angular momentum vs. energy (top panel), and vs. the perpendicular component of the angular momentum (bottom panel). The location of *Gaia* BH3 is indicated with a cross and falls right on top of the ED-2 stream members. Note that the values of the IoM were computed in the Milky Way potential of Dodd et al. (2023), which is slightly different from that used in Gaia Collaboration: Panuzzo et al. (2024). The Mahalanobis distance<sup>2</sup> between the

<sup>2</sup> The Mahalanobis distance between BH3 and ED-2 (Sequoia) is defined as  $D_{BH3}^2 = (\mu_i - \mu_{BH3})^T \Sigma_i^{-1} (\mu_i - \mu_{BH3})$  where  $\mu_{BH3}$  denotes the

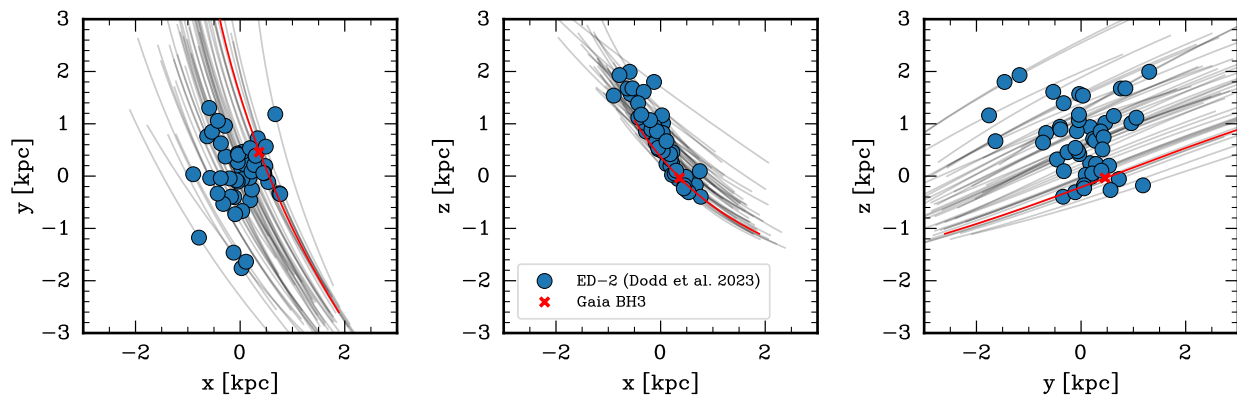


**Fig. 3.** Cartesian heliocentric projection of the location of ED-2 members and their orbits integrated in the Milky Way potential used in Dodd et al. (2023) for 20 Myr. The red cross and line show the position and orbit of *Gaia* BH3, and is indistinguishable from that of the ED-2 stars.

centre of ED-2 and *Gaia* BH3 is 0.942, while that between Sequoia and *Gaia* BH3 is 2.718. In other words, only 17% of the members of ED-2 are closer to its centre than *Gaia* BH3, while it is in the outskirts of Sequoia as 94% of its stars have a smaller distance. This makes it much more likely that *Gaia* BH3 is associated to ED-2 than to Sequoia.

This is further illustrated by the trajectories followed by the stars in ED-2 and *Gaia* BH3 shown in Fig. 3, where there is no noticeable distinction between the different objects. It is interesting that BH3 is not at the centre of the distribution of stars. Whether this is real or due to incompleteness in the sample (i.e. the distance limit and the magnitude limit of the RVS dataset) should be scrutinised in-depth in further studies.

Given the size of the ED-2 structure in IoM space, which is rather comparable to that of other globular clusters, such as NGC3201 and NGC6101 also shown in Fig. 2, we tentatively conclude that ED-2 stems from a GC-like progenitor. The good fit obtained from a single stellar population further supports this conclusion.

### 3. Chemical abundances

We obtained spectra for 3 stars as part of the follow-up of the ED-2 stream in period 111 (April – September 2023; proposal submitted in September 2022) with the optical spectrograph, UVES (Dekker et al. 2000) mounted at the Very Large Telescope (VLT) of the European Southern Observatory (ESO). We have also used ESO archival data for another ED-2 member, source\_ID 4479226310758314496. Additionally, we observed 6 ED-2 core members with X-Shooter (Vernet et al. 2011) at the VLT in period 112 (October 2023 – March 2024; proposal submitted in March 2023). In all cases, we used the phase-3 data products provided by ESO for further analysis. In the Appendix we provide details of the observational set-ups, and we also describe the procedure used to derive the stellar parameters and chemical abundances of the UVES stars and the [Fe/H] for the X-Shooter targets. We list the results in Table A.1 and Table A.2 for the stars observed with UVES and X-shooter respectively.

Fig. 4 shows the metallicity distribution derived for the ED-2 stars in our programs. The top panel corresponds to the UVES targets whose metallicity is measured from the Fe II lines, which are more reliable due to their small sensitivity to the adopted stellar parameters and non-LTE effects. The middle panels are

location of BH3 in IoM space and  $\mu_i$  and  $\Sigma_i$  are the mean and covariance matrix of the ED-2 (Sequoia) stars.

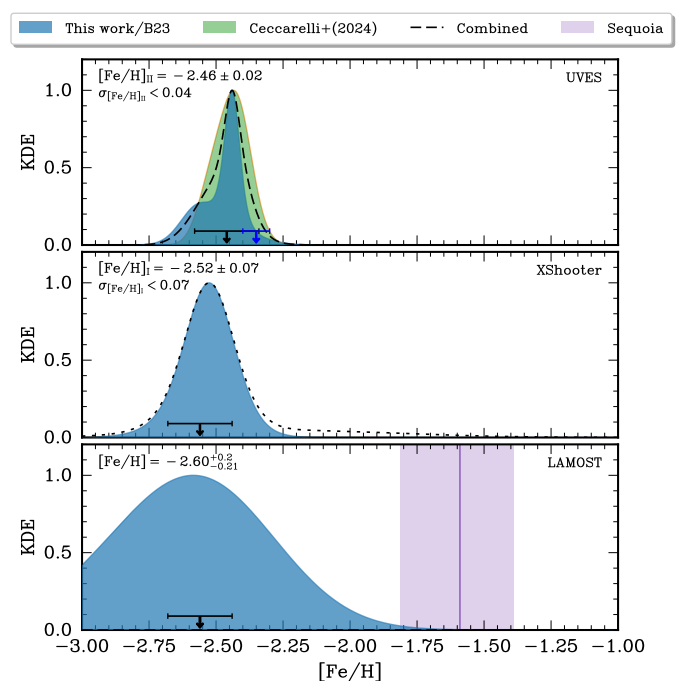


**Fig. 4.** Metallicity distribution for ED-2 based on UVES, X-Shooter and LAMOST spectra in the top, middle and bottom panels respectively. The arrow and errorbar show *Gaia* BH3’s companion’s metallicity and uncertainty, as inferred by *Gaia* Collaboration: Panuzzo et al. (2024), and in the top panel, using Fe II lines and by our own analysis in blue (see also Table A.1). In the top left of each panel the best-fit metallicity and the upper bound on the metallicity dispersion are given. In the middle panel, the dashed distribution includes a star with large [Fe/H] uncertainties. We also show in the bottom panel the 25%–75% quantiles for members of Sequoia (following the classification of Dodd et al. 2023) as a shaded band using metallicity estimates from LAMOST.

for the X-Shooter stars, while the bottom panel shows the distribution derived by B23 compared to that of Sequoia as defined by Dodd et al. (2023), both using LAMOST spectra. The black arrow and errorbar show *Gaia* BH3 visible companion’s metallicity and its uncertainty. This figure confirms, now on the basis of the metallicity, that the black hole is a member of ED-2, and has a negligible probability to be part of Sequoia.

We measure the mean metallicity and metallicity dispersion ( $\sigma_{[\text{Fe}/\text{H}],int}$ ) of ED-2 in the UVES and X-Shooter samples assum-

ing a simple normal distribution with dispersion  $\sigma^2 = \sigma_{[\text{Fe}/\text{H}],\text{int}}^2 + \sigma_{[\text{Fe}/\text{H}],j}^2$ , i.e. the sum in quadrature of an intrinsic dispersion and the metallicity uncertainty in each  $j$ -th data point. We use this distribution to maximize the likelihood of our model using EMCEE (Foreman-Mackey et al. 2013). For the UVES sample, we find a best-fit metallicity of  $[\text{Fe}/\text{H}]_{\text{II}} = -2.46 \pm 0.02$  and a metallicity dispersion  $\sigma_{[\text{Fe}/\text{H}]} < 0.04$ . Similarly, for the X-Shooter sample, we find a best-fit metallicity of  $[\text{Fe}/\text{H}] = -2.51 \pm 0.07$  and a metallicity dispersion  $\sigma_{[\text{Fe}/\text{H}]} < 0.07^3$ . The uncertainties in metallicity were computed from the standard deviation of the posterior distribution, while the upper limits in  $\sigma_{[\text{Fe}/\text{H}]}$  are the 67% quantile of the posterior. We thus find that the intrinsic metallicity dispersion of ED-2 is consistent with zero. This favours a star cluster origin as opposed to a dwarf galaxy, as even ultra-faint dwarfs have a scatter of at least 0.3 dex (Simon 2019).

Fig. 5 shows the abundances of Mg, Na and Al with respect to Fe for the stars observed with UVES (blue triangles). The scatter in all elements is very small, again indicating that the ED-2 originated in a star cluster. Also the abundances measured for other ED-2 stars by Ceccarelli et al. (2024, green diamonds) show very comparable values. The measurements for the companion star of *Gaia* BH3 as provided by *Gaia* Collaboration: Panuzzo et al. (2024, in orange) and by our own analysis (in red) are shown with a cross symbol, and are fully consistent with those of the ED-2 stars. Also its measured  $[\text{Eu}/\text{Fe}] = 0.52$  is in excellent agreement with that of another star in ED-2, for which we could measure  $[\text{Eu}/\text{Fe}] = 0.61$ , a value that supports similar amounts of r-process enhancement across the system. ED-2's mean abundance of  $[\text{Ba}/\text{Fe}] = 0.22$  (and its small dispersion of 0.1 dex) is consistent with that of other halo stars, but different from that seen in ultra-faint dwarf galaxies, which typically depict much larger or much lower values (Ji et al. 2019). In Fig. 5 we plotted for comparison the abundances of a set of GCs from Carretta et al. (2009, all of which are more metal-rich), which reveal a similar scatter in  $[\text{Mg}/\text{Fe}]$  as ED-2 members but larger in Na and Al.

The low  $[\text{Al}/\text{Fe}]$  and high  $[\text{Mg}/\text{Mn}]$  of the ED-2 stars and of the companion star of *Gaia* BH3 (see Table A.1) places ED-2 members in a region of abundance-space that is referred to as “chemically unevolved” (Hawkins et al. 2015; Fernandes et al. 2023). This could hint at an accretion origin of ED-2 given also its highly retrograde orbit. However, care must be taken when interpreting this chemical space since its validity as an indicator of a possible accretion origin has not been firmly established for star clusters.

#### 4. Discussion

Having established that *Gaia* BH3 formed in a star cluster, we now explore possible formation channels. We also attempt to infer some properties of the ED-2 parent cluster. Note that these findings naturally explain the “normal” chemical composition of its accompanying star, in the sense that the binary could easily have formed in the cluster after the BH was born.

The most straightforward formation scenario for BHs is through the collapse of a very massive star. The mass of such a BH is dictated by the star's mass at the end of its evolution. Due to the details of the mass-loss process, this can differ significantly from its initial value. Using the single-star initial-final

<sup>3</sup> Although the star with source\_ID 3757312745743087232 is more metal-rich than the remainder of the sample (see Table A.2), it has very large uncertainties, and its inclusion has no effect in the derived mean and spread in metallicity.

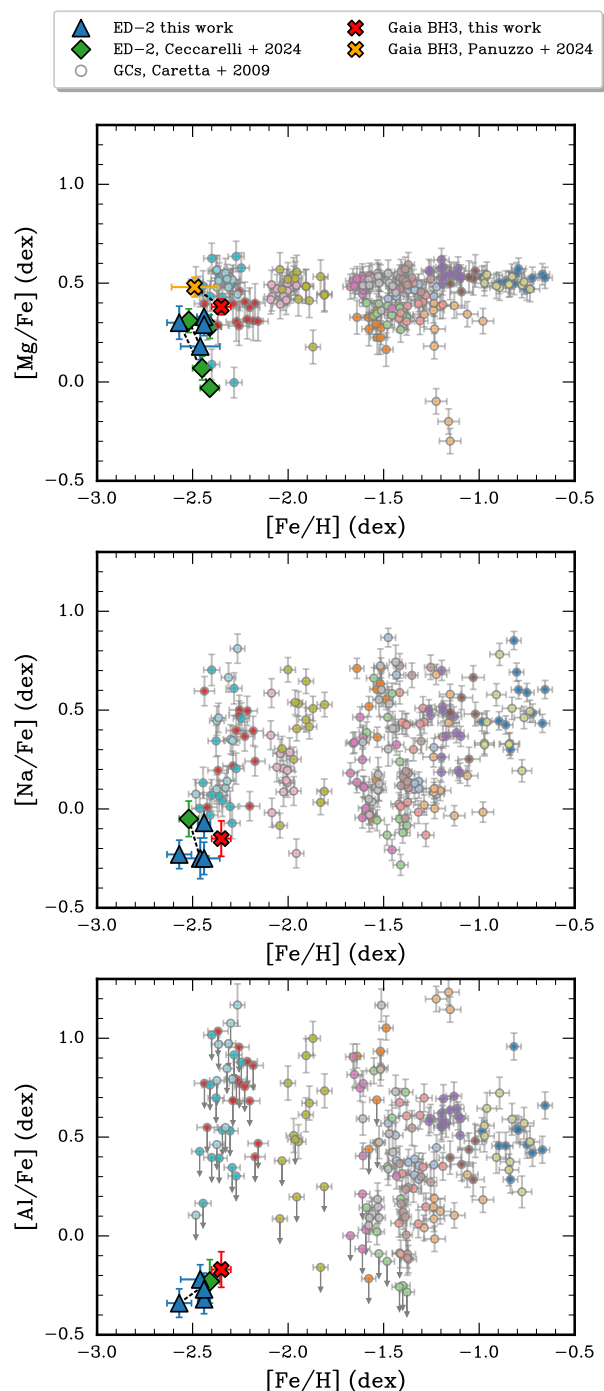


**Fig. 5.** Abundances of Mg/Fe, Na/Fe and Al/Fe for the 4 ED-2 stars in our UVES sample (blue triangles), and for ED-2 stars from Ceccarelli et al. (2024, green diamonds). Note the good agreement and small scatter. Also chemically the companion of *Gaia* BH3 (cross symbol, red corresponds to our own abundances and orange to the measurements from *Gaia* Collaboration: Panuzzo et al. (2024), see also Table A.1) is indistinguishable from ED-2 stars (see also text). For comparison, we have plotted also (upper limits to) the abundances for several GCs from Carretta et al. (2009).

mass relations (IFMR) from Fryer et al. (2012) implemented in `ssptools`<sup>4</sup> (Balbinot & Gieles 2018; Dickson et al. 2023) and a Kroupa initial mass function, we can infer how many stellar BHs of a given mass are likely to form as a function of the clus-

<sup>4</sup> <https://github.com/SMU-clusters/ssptools>

ter mass. We find that the minimum mass for a star cluster to host at least 1 stellar BH of the size of *Gaia* BH3 or higher is  $M_{\text{cl,min}} \approx 2 \times 10^3 M_{\odot}$ . In this case, *Gaia* BH3 would be a first generation BH.

Alternative pathways to produce very massive BHs have been proposed that require binary evolution and dynamical hardening of these binary systems. These processes take place in dense stellar systems such as GCs (see e.g. Portegies Zwart & McMillan 2000), and see also the recent work on young star clusters by Rastello et al. (2023); Tanikawa et al. (2024); Di Carlo et al. (2024). Due to their stochastic nature, such processes can produce BH with a wide range of masses (see e.g. Antonini & Gieles 2020). In this case, *Gaia* BH3 could have formed via the mergers of subsequent generations of BHs.

The scatter in the Na and Al abundances seen in GCs is indicative of multiple stellar populations and has a dependence on both mass and metallicity (see e.g. Gratton et al. 2019). Fnx I, a GC in the Fornax dwarf spheroidal, has  $[\text{Fe}/\text{H}] \approx 2.5$ , and does show multiple populations, as well as scatter in  $[\text{Na}/\text{Fe}]$  (Letarte et al. 2006), and its initial mass has been estimated to be  $4.2 \times 10^4 M_{\odot}$  by de Boer & Fraser (2016). Therefore, the (near) lack of such a scatter for ED-2 suggests its parent cluster was lighter in mass than Fnx I. We may also use the relationship by Pancino et al. (2017) between the spread in  $[\text{Al}/\text{Fe}]$ , the mean  $[\text{Fe}/\text{H}]$  of the cluster and its mass:  $\Delta[\text{Al}/\text{Mg}] = 0.67(0.21) \log M_{\text{cl}} - 0.53(0.17)[\text{Fe}/\text{H}] - 3.16(1.11)$ . By randomly drawing  $[\text{Al}/\text{Mg}]$  for each star within the uncertainties, we obtain a distribution of  $\Delta[\text{Al}/\text{Mg}]$ , and considering the uncertainties in the coefficients in a similar fashion, we can infer a distribution of possible cluster masses. We find a median value of  $\log M_{\text{cl}}/M_{\odot} = 2.86$ , with the 25% and 75% quantiles of  $\log M_{\text{cl}}/M_{\odot}$  being 1.68 and 4.33 respectively. If the scatter is only due to errors, this estimate would be an upper limit. It is however based on an extrapolation of a relation determined for Galactic clusters whose metallicities are all higher than ED-2's, and whose present-day masses could differ from their initial values by at least a factor of 2 (Anders et al. 2009). Nevertheless, it is reassuring that this upper limit is consistent with that provided by the comparison to Fnx I.

Further support for ED-2 having been a low-mass star cluster comes from the fact that the *Gaia* BH3 system is a relatively wide binary, with a period of 11.6 yr. Such long period binaries do not survive in massive GCs because they are either quickly disrupted or become tighter because of interactions within such systems (Ivanova et al. 2005, although its low mass-ratio enhances the chances of survival). Unlike NGC6101 or NGC3201, the two GC with similar orbits plotted in Fig. 2, ED-2 did not manage to survive as a star cluster until the present day. This could be due to its lower mass or a lower density. But also the retention of *Gaia* BH3 by the ED-2 cluster could have contributed in speeding-up its disruption (Gieles et al. 2021).

## 5. Conclusions

In this Letter, we have shown that the  $33 M_{\odot}$  black hole *Gaia* BH3 is associated to the ED-2 retrograde halo stellar stream. The BH's orbit around the Galaxy is indistinguishable from that of ED-2 members. Using high-resolution spectra of ED-2 stars, we have determined that ED-2's mean metallicity is entirely consistent with that of the companion of *Gaia* BH3, as are other chemical elemental abundances such as  $[\text{Mg}/\text{Fe}]$ ,  $[\text{Eu}/\text{Fe}]$  and  $[\text{Ba}/\text{Fe}]$ . Furthermore, we have shown that the metallicity spread in ED-2 is consistent with zero, indicating that it stems from a disrupted star cluster. This is entirely in-line with its colour-magnitude di-

agram, which is very well fit by an extremely old single stellar population, similar to that of the GC M92, indicating that the progenitor of *Gaia* BH3 formed more than 13 Gyr ago. The (near) lack of scatter in Na and Al suggests that ED-2's parent system was a small cluster with mass smaller than  $4.2 \times 10^4 M_{\odot}$ . This would leave a small window for *Gaia* BH3 to be the direct result of the collapse of a massive star, since we have found that such a heavy BH can only form in a system more massive than  $2 \times 10^3 M_{\odot}$ . To shed more light on its formation channels, sophisticated dynamical models of the ED-2 parent cluster, including stellar evolution and binary interactions, and using as boundary conditions those inferred in this paper (e.g. mass range, metallicity, and orbit) are needed. Furthermore, the mapping of the ED-2 stream beyond the Solar neighbourhood would allow a reliable and independent determination of the initial cluster mass. Finally, detailed chemical abundances for more of its members would put a tighter constraint on the lack of a spread of light elements and constrain further the evolution of the system.

*Acknowledgements.* The authors would like to thank Elena Pancino and Mark Gieles for the insightful discussion on GC chemistry and BH evolution, and Gijs Nelemans for useful references. We acknowledge support from a Spinoza prize from the Netherlands Organisation for Scientific Research (NWO). TM is supported by a Gliese Fellowship at the Zentrum für Astronomie, University of Heidelberg, Germany. This study was supported by the Klaus Tschira Foundation. We have made use of data from the European Space Agency (ESA) mission *Gaia* (<https://www.cosmos.esa.int/gaia>), processed by the *Gaia* Data Processing and Analysis Consortium (DPAC, <https://www.cosmos.esa.int/web/gaia/dpac/consortium>). Funding for the DPAC has been provided by national institutions, in particular the institutions participating in the *Gaia* Multilateral Agreement. Non-public data underlying this article will be shared on reasonable request to the authors. Based on observations made with ESO Telescopes at the La Silla Paranal Observatory under programme ID 112.25ZW.001 (PI: Balbinot), 111.2537.001 (PI: Dodd), and 106.21JJ.001 (PI: Matsuno). The following software packages were used in this publication: *Astropy* (Astropy Collaboration et al. 2013, 2018), *dustmaps* (Green 2018), *IPython* (Pérez & Granger 2007), *matplotlib* (Hunter 2007), *numpy* (Walt et al. 2011), *scipy* (Jones et al. 2001–), *vaex* (Breddels & Veljanoski 2018)

## References

- Abbott, R., Abbott, T. D., Acernese, F., et al. 2023a, *Physical Review X*, 13, 041039
- Abbott, R., Abbott, T. D., Acernese, F., et al. 2023b, *Physical Review X*, 13, 011048
- Anders, P., Lamers, H. J. G. L. M., & Baumgardt, H. 2009, *A&A*, 502, 817
- Andrae, R., Rix, H.-W., & Chandra, V. 2023, arXiv e-prints, arXiv:2302.02611
- Antonini, F. & Gieles, M. 2020, *MNRAS*, 492, 2936
- Astropy Collaboration, Price-Whelan, A. M., Sipőcz, B. M., et al. 2018, *AJ*, 156, 123
- Astropy Collaboration, Robitaille, T. P., Tollerud, E. J., et al. 2013, *A&A*, 558, A33
- Balbinot, E. & Gieles, M. 2018, *MNRAS*, 474, 2479
- Balbinot, E., Helmi, A., Callingham, T., et al. 2023, *A&A*, 678, A115
- Breddels, M. A. & Veljanoski, J. 2018, *A&A*, 618, A13
- Carretta, E., Bragaglia, A., Gratton, R., & Lucatello, S. 2009, *A&A*, 505, 139
- Casagrande, L. & Vandenberg, D. A. 2014, *MNRAS*, 444, 392
- Ceccarelli, E., Massari, D., Mucciarelli, A., et al. 2024, *A&A*, 684, A37
- Clementini, G., Ripepi, V., Garofalo, A., et al. 2023, *A&A*, 674, A18
- de Boer, T. J. L. & Fraser, M. 2016, *A&A*, 590, A35
- Dekker, H., D'Odorico, S., Kaufer, A., Delabre, B., & Kotzlowski, H. 2000, in *Society of Photo-Optical Instrumentation Engineers (SPIE) Conference Series*, Vol. 4008, *Optical and IR Telescope Instrumentation and Detectors*, ed. M. Iye & A. F. Moorwood, 534–545
- Di Carlo, U. N., Agrawal, P., Rodriguez, C. L., & Breivik, K. 2024, *ApJ*, 965, 22
- Dickson, N., Hénault-Brunet, V., Baumgardt, H., Gieles, M., & Smith, P. J. 2023, *MNRAS*, 522, 5320
- Dodd, E., Callingham, T. M., Helmi, A., et al. 2023, *A&A*, 670, L2
- Fernandes, L., Mason, A. C., Horta, D., et al. 2023, *MNRAS*, 519, 3611
- Foreman-Mackey, D., Hogg, D. W., Lang, D., & Goodman, J. 2013, *PASP*, 125, 306
- Fragione, G. & Rasio, F. A. 2023, *ApJ*, 951, 129
- Fryer, C. L., Belczynski, K., Wiktorowicz, G., et al. 2012, *ApJ*, 749, 91

- Gaia Collaboration: Panuzzo, Mazeh, T., & et al., . 2024, A&A
- Gieles, M., Erkal, D., Antonini, F., Balbinot, E., & Peñarrubia, J. 2021, *Nature Astronomy*, 5, 957
- Gratton, R., Bragaglia, A., Carretta, E., et al. 2019, *A&A Rev.*, 27, 8
- Green, G. 2018, *The Journal of Open Source Software*, 3, 695
- Green, G. M., Schlafly, E., Zucker, C., Speagle, J. S., & Finkbeiner, D. 2019, *ApJ*, 887, 93
- Gustafsson, B., Edvardsson, B., Eriksson, K., et al. 2008, *A&A*, 486, 951
- Hawkins, K., Jofré, P., Masseron, T., & Gilmore, G. 2015, *MNRAS*, 453, 758
- Hunter, J. D. 2007, *Computing in Science and Engineering*, 9, 90
- Ivanova, N., Belczynski, K., Fregeau, J. M., & Rasio, F. A. 2005, *MNRAS*, 358, 572
- Ji, A. P., Simon, J. D., Frebel, A., Venn, K. A., & Hansen, T. T. 2019, *ApJ*, 870, 83
- Jones, E., Oliphant, T., Peterson, P., et al. 2001–, *SciPy: Open source scientific tools for Python*
- Kupka, F., Dubernet, M. L., & VAMDC Collaboration. 2011, *Baltic Astronomy*, 20, 503
- Kurucz, R. L. 2005, *Memorie della Societa Astronomica Italiana Supplementi*, 8, 14
- Lallement, R., Vergely, J. L., Babusiaux, C., & Cox, N. L. J. 2022, *A&A*, 661, A147
- Letarte, B., Hill, V., Jablonka, P., et al. 2006, *A&A*, 453, 547
- Li, H., Tan, K., & Zhao, G. 2018, *ApJS*, 238, 16
- Lind, K., Nordlander, T., Wehrhahn, A., et al. 2022, *A&A*, 665, A33
- M. Kovalev, S. Brinkmann, M. Bergemann, & MPIA IT-department. 2018, NLTE MPIA web server, [Online]. Available: <http://nlte.mpia.de> Max Planck Institute for Astronomy, Heidelberg.
- Matsuno, T., Aoki, W., & Suda, T. 2019, *ApJ*, 874, L35
- Mucciarelli, A., Bellazzini, M., & Massari, D. 2021, *A&A*, 653, A90
- Myeong, G. C., Vasiliev, E., Iorio, G., Evans, N. W., & Belokurov, V. 2019, *MNRAS*, 488, 1235
- Naidu, R. P., Conroy, C., Bonaca, A., et al. 2020, *ApJ*, 901, 48
- Pancino, E., Romano, D., Tang, B., et al. 2017, *A&A*, 601, A112
- Pérez, F. & Granger, B. E. 2007, *Computing in Science and Engineering*, 9, 21
- Portegies Zwart, S. F. & McMillan, S. L. W. 2000, *ApJ*, 528, L17
- Rastello, S., Iorio, G., Mapelli, M., et al. 2023, *MNRAS*, 526, 740
- Ruiz-Lara, T., Matsuno, T., Lövdal, S. S., et al. 2022, *A&A*, 665, A58
- Sbordone, L., Bonifacio, P., Castelli, F., & Kurucz, R. L. 2004, *Memorie della Societa Astronomica Italiana Supplementi*, 5, 93
- Schlegel, D. J., Finkbeiner, D. P., & Davis, M. 1998, *ApJ*, 500, 525
- Simon, J. D. 2019, *ARA&A*, 57, 375
- Snedden, C. A. 1973, PhD thesis, University of Texas, Austin
- Tanikawa, A., Cary, S., Shikauchi, M., Wang, L., & Fujii, M. S. 2024, *MNRAS*, 527, 4031
- Vasiliev, E. & Baumgardt, H. 2021, *MNRAS*, 505, 5978
- Vernet, J., Dekker, H., D’Odorico, S., et al. 2011, *A&A*, 536, A105
- Walt, S. v. d., Colbert, S. C., & Varoquaux, G. 2011, *Computing in Science and Engg.*, 13, 22
- Ying, J. M., Chaboyer, B., Boudreux, E. M., et al. 2023, *AJ*, 166, 18
- <sup>12</sup> Astronomical Observatory, University of Warsaw, Al. Ujazdowskie 4, 00-478 Warszawa, Poland
- <sup>13</sup> HE Space Operations BV for European Space Agency (ESA), Camino bajo del Castillo, s/n, Urbanización Villafranca del Castillo, Villanueva de la Cañada, 28692 Madrid, Spain
- <sup>14</sup> Mullard Space Science Laboratory, University College London, Holmbury St Mary, Dorking, Surrey RH5 6NT, United Kingdom
- <sup>15</sup> Telespazio UK S.L. for European Space Agency (ESA), Camino bajo del Castillo, s/n, Urbanización Villafranca del Castillo, Villanueva de la Cañada, 28692 Madrid, Spain
- <sup>16</sup> Universidad de Granada, Departamento de Física Teórica y del Cosmos, Campus Fuente Nueva, Edificio Mecenaz, E-18071, Granada, Spain
- <sup>17</sup> Instituto Carlos I de Física Teórica y computacional, Universidad de Granada, E-18071 Granada, Spain

<sup>1</sup> Kapteyn Astronomical Institute, University of Groningen, Landleven 12, 9747 AD Groningen, The Netherlands

<sup>2</sup> Leiden Observatory, Leiden University, Einsteinweg 55, 2333 CC Leiden, The Netherlands

<sup>3</sup> Astronomisches Rechen-Institut, Zentrum für Astronomie der Universität Heidelberg, Mönchhofstr. 12-14, 69120 Heidelberg, Germany

<sup>4</sup> Dipartimento di Fisica e Astronomia, Università degli Studi di Bologna, Via Gobetti 93/2, I-40129 Bologna, Italy

<sup>5</sup> GEPI, Observatoire de Paris, Université PSL, CNRS, 5 Place Jules Janssen, 92190 Meudon, France

<sup>6</sup> School of Physics and Astronomy, Tel Aviv University, Tel Aviv 6997801, Israel

<sup>7</sup> Department of Astronomy, University of Geneva, Chemin Pegasi 51, 1290 Versoix, Switzerland

<sup>8</sup> Department of Astronomy, University of Geneva, Chemin d’Ecogia 16, 1290 Versoix, Switzerland

<sup>9</sup> Institut d’Astronomie et d’Astrophysique, Université Libre de Bruxelles CP 226, Boulevard du Triomphe, 1050 Brussels, Belgium

<sup>10</sup> Univ. Grenoble Alpes, CNRS, IPAG, 38000 Grenoble, France

<sup>11</sup> RHEA for European Space Agency (ESA), Camino bajo del Castillo, s/n, Urbanización Villafranca del Castillo, Villanueva de la Cañada, 28692 Madrid, Spain

## Appendix A: Derivation of stellar parameters and chemical abundances of ED-2 stars

We obtained spectra for 3 stars as part of the follow-up of the ED-2 stream in period 111 (April – September 2023; proposal submitted in September 2022; program 0111.D-0263(A), PI:Dodd) with the optical spectrograph, UVES mounted at the Very Large Telescope (VLT) of the European Southern Observatory. The observations were performed with UVES in Dichroic mode adopting the standard settings Dic 1 Blue Arm CD2 390 (326–454 nm) and Dic 1 Red Arm CD3 580 (476–684 nm) and with the 0.7'' slit width, thus yielding a resolution of  $R \approx 55000$ , and  $S/N \approx 15$  for the Blue Arm and  $S/N \approx 30$  for the Red Arm on average. We have also used ESO archival data from the programs 0109.B-0522(A) and 167.D-0173(A), for another ED-2 member, source\_ID 4479226310758314496. Additionally, we observed 7 ED-2 stars with X-Shooter at the VLT in period 112 (October 2023 – March 2024; proposal submitted in March 2023; program 112.25ZW.001; PI: Balbinot). In all cases, we used the phase 3 data products provided by ESO for further analysis.

For the UVES spectra we derived the chemical abundances of the stars using the 1D LTE spectral synthesis code MOOG (Snedden 1973) with the grid of MARCS model atmospheres (Gustafsson et al. 2008). Stellar parameters ( $T_{\text{eff}}$  and  $\log g$ ) were determined from dereddened photometry and astrometry;  $T_{\text{eff}}$  was obtained from the  $G - K_s$  color using the relation from Mucciarelli et al. (2021), and  $\log g$  was obtained from the  $K_s$  magnitude together with the bolometric correction of Casagrande & Vandenberg (2014) and an assumption of a mass of  $0.8 M_{\odot}$ . The extinction was taken from Green et al. (2019) where available and Schlegel et al. (1998) otherwise. We measured abundances of Mg and Fe through equivalent widths analysis and of Na, Al, Mn, Ba, and Eu through spectral synthesis with hyperfine structure splitting included, and applied non-LTE corrections of Lind et al. (2022) to the Na and Al abundances. We simply averaged the line-by-line abundances to obtain the final abundance of each element. We estimate the uncertainties from the sample standard deviation of the line-by-line abundances ( $\sigma$ ) and the number of lines ( $N$ ) as  $\sigma / \sqrt{N}$  when  $N > 3$ ; otherwise, we replace the  $\sigma$  with that of neutral iron. We additionally consider the uncertainties due to the stellar parameters. We report the measured abundances in Table A.1.

For the X-Shooter spectra, we initially stack individual radial velocity corrected exposures. We assume atmospheric parameters from Andrae et al. (2023), with the exception of star 3757312745743087232, where *Gaia* XP spectra was used instead. We synthesised  $H\alpha$  and  $H\beta$  non-local thermodynamic equilibrium (NLTE) line profiles using the tools provided by M. Kovalev et al. (2018). We find that the adopted values for  $T_{\text{eff}}$  and  $\log(g)$  adequately reproduce the wings of the Balmer lines. The spectra for each star was normalized assuming a  $[\text{Fe}/\text{H}] = -2.5$  template in the range between 330nm to 1100nm. Finally, while keeping the atmospheric parameters constant we derived Fe abundances using the SYNTHE transfer code (Sbordone et al. 2004), assuming the ATLAS 9 models (Kurucz 2005), and atomic data from Kupka et al. (2011). We do so by minimising the  $\chi^2$  between observed and synthetic fluxes around a set of selected Fe features. We report the Fe abundances and their associated uncertainty in Table A.2.

**Table A.1.** Stellar parameters and chemical abundances for ED-2 stars. The 3 ED-2 stars in our UVES program, supplemented by an ED-2 star from the ESO archive (second entry) are shown in the first part. The bottom two entries correspond to the binary star of *Gaia* BH3, as estimated following the procedure described in this paper and as presented in [Gaia Collaboration: Panuzzo et al. \(2024\)](#), respectively.

| source_id                              | $T_{\text{eff}}$<br>[K] | log $g$<br>– | $v_r$<br>[km s <sup>-1</sup> ] | [Fe/H] <sub>I</sub><br>– | [Fe/H] <sub>II</sub><br>– | [Na/Fe]<br>– | [Mg/Fe]<br>– | [Al/Fe]<br>– | [Mn/Fe]<br>– | [Ba/Fe]<br>– | [Eu/Fe]<br>– |       |      |       |      |       |      |      |      |
|--|-------------------------|--------------|--------------------------------|--------------------------|---------------------------|--------------|--------------|--------------|--------------|--------------|--------------|-------|------|-------|------|-------|------|------|------|
| 4245522468554091904                    | 6657                    | 4.30         | 1.68                           | -2.48                    | 0.05                      | -2.46        | 0.10         | -0.25        | 0.10         | 0.18         | 0.07         | -0.22 | 0.07 | -0.45 | 0.12 | -0.13 | 0.15 |      |      |
| 4479226310758314496                    | 5974                    | 4.53         | 1.12                           | -2.70                    | 0.05                      | -2.57        | 0.06         | -0.23        | 0.07         | 0.30         | 0.08         | -0.34 | 0.07 | -0.52 | 0.09 | -0.35 | 0.10 |      |      |
| 6632335060231088896                    | 5620                    | 3.60         | 1.32                           | -2.54                    | 0.05                      | -2.44        | 0.04         | -0.07        | 0.08         | 0.33         | 0.06         | -0.32 | 0.07 | -0.41 | 0.06 | -0.17 | 0.08 | 0.61 | 0.08 |
| 6746114585056265600                    | 6110                    | 4.55         | 1.28                           | -2.57                    | 0.05                      | -2.44        | 0.02         | -0.25        | 0.08         | 0.29         | 0.06         | -0.27 | 0.08 | -0.43 | 0.06 | -0.24 | 0.09 |      |      |
| <b>4318465066420528000<sup>a</sup></b> | 5445                    | 3.04         | 1.60                           | -2.33                    | 0.05                      | -2.35        | 0.05         | -0.15        | 0.09         | 0.38         | 0.04         | -0.17 | 0.09 | -0.14 | 0.10 | -0.04 | 0.10 | 0.58 | 0.10 |
| <b>4318465066420528000<sup>a</sup></b> | 5211                    | 2.93         | 1.19                           | -2.56                    | 0.12                      | -2.49        | 0.12         |              |              | 0.48         | 0.05         |       |      |       |      | 0.11  | 0.13 | 0.52 | 0.05 |

**Notes.** <sup>(a)</sup> We note that the difference  $T_{\text{eff}}$  between the two studies is due to different extinction maps used and is responsible for the relatively large difference in  $[\text{Fe}/\text{H}]_I$ . The differences in the other ratios are likely due to systematic errors that are not accounted for in the quoted uncertainties, as the abundance ratios are rather insensitive to the choice of  $T_{\text{eff}}$ . Sources for such systematic uncertainties include the use of different linelists, radiative transfer codes, and atmospheric models.

**Table A.2.** Stellar parameters and  $[\text{Fe}/\text{H}]$  for the X-Shooter sample. The reported  $T_{\text{eff}}$  and log  $g$  are from [Andrae et al. \(2023\)](#), except for star source\_id 3757312745743087232 where the atmospheric parameters were inferred from the *Gaia* XP spectra. We add a <sup>a</sup> to the source\_id to mark stars not original in [Dodd et al. \(2023\)](#).

| source_id            | $T_{\text{eff}}$<br>[K] | log $g$<br>– | [Fe/H] <sub>I</sub><br>– |      |
|----------------------|-------------------------|--------------|--------------------------|------|
| 3549718318990080896  | 5319                    | 3.3          | -2.52                    | 0.08 |
| 3869876996687740032* | 5372                    | 3.4          | -2.50                    | 0.10 |
| 6747065215934660608  | 5535                    | 4.3          | -2.53                    | 0.08 |
| 6646097819069706624  | 5653                    | 4.4          | -2.54                    | 0.10 |
| 3473979147705211776  | 5733                    | 4.4          | -2.57                    | 0.14 |
| 3757312745743087232  | 6591                    | 4.2          | -2.23                    | 0.41 |